14th International Conference on Applications of Statistics and Probability in Civil Engineering, ICASP14
Dublin, Ireland, July 9-13, 2023

Adaptive Learning for Surrogate Models in Active Subspace for High Dimensional Problems

Yulin Guo
Graduate Student, Dept. of Civil and Environmental Engineering, Vanderbilt University, Nashville, TN, USA

Paromita Nath
Assistant Professor, Dept. of Mechanical Engineering, Rowan University, Glassboro, NJ, USA

Sankaran Mahadevan
Professor, Dept. of Civil and Environmental Engineering, Vanderbilt University, Nashville, TN, USA

ABSTRACT: Surrogate models are often employed in engineering analysis to replace a detailed model with complicated geometry, loading, material properties and boundary conditions, in order to achieve computational efficiency in iterative calculations such as model calibration or design optimization. The accuracy of the surrogate model depends on the quality and quantity of data collected from the expensive physics-based model. This paper presents a novel approach to efficiently construct and improve surrogate models for high dimensional problems in both the input and output spaces. In the proposed method, the principal components and corresponding features in the output field quantity are first identified. Mapping between inputs and each feature is then considered, and the active subspace methodology is used to capture the relationship in a low-dimensional subspace in the input domain. Thus dimension reduction is accomplished in both the input and output spaces, and surrogate models are built within the reduced spaces. A new low-dimensional adaptive learning strategy is proposed in this work to improve the surrogate model. With multiple iterations of this adaptive learning procedure, the optimal surrogate is achieved without intensive model simulations. In contrast to existing adaptive learning methods which focus on scalar output or a limited number of output quantities, this paper addresses adaptive learning for both high-dimensional input and output, with a novel learning function balancing exploration and exploitation. The adaptive learning is based on the active variables in the low-dimensional space and once the newly-added training sample is selected, it can be easily mapped back to the original space for running the physics-based model. The proposed method is demonstrated on an additively manufactured component, with a high-dimensional field output quantity of interest, namely the residual stress in the component that has spatial variability due to the stochastic nature of multiple input variables (including process variables and material properties).

1. INTRODUCTION

Engineering analysis such as reliability analysis, model calibration, and design optimization typically requires evaluations of the physics-based computation models at tens of thousands of samples in the input space. It is expensive to run the detailed physics-based models for a large number of times. For complex systems, the quantities of interest can be a multivariate output, which may be spatially or temporally correlated, and a function of a large

set of variables in the input space. In order to address the challenges posed by computational costs, correlations, and high dimensionalities in both input and output spaces, inexpensive surrogate models are necessary to replace the expensive models to efficiently map the model input to the output. The accuracy of the surrogate model depends on the quality and quantity of data collected from the expensive physics-based model, it is computationally expensive itself to construct a surrogate model and iteratively improve it to a reasonably accuracy level by active learning, especially in the context of high dimensional multi-physics problems. For high dimensional problems, a large number of samples are required for sufficient surrogate modeling. It is also crucial to conduct efficient design of experiments (Sacks et al. (1989)), or DoE, for accurate surrogate model construction with minimal computational cost. Non-adaptive DoE methods may result in unsatisfactory surrogate models due to the lack of prior knowledge of the target function and limited computational resources; adaptive DoE methods use an active learning-based sampling strategies that utilize information of existing samples and the surrogate model in the previous iteration, thus new samples can be sequentially added in regions where the target function is nonlinear or exhibits drastic change.

Most studies focus on efficiency improvement by lowering the dimensionality in either the input space or the output space. Recent work has considered both input and output dimension reduction, such as the principal component-active subspace (PCAS) method (Vohra et al. (2020); White et al. (2019)), but limited to tens of inputs and hundreds of outputs; in Guo et al. (2022), a systematic way of finding the most suitable methods for the surrogate modeling for high-dimensional problems based on the size of dimensionality is proposed. Recent work also investigate adaptive learning strategies, however, they focus on a limit state rather than a function over the entire input space, and focus on a scalar output with limited number of input.

In this paper, we aim to address the adaptive surrogate modeling for problems with high dimensionalities in both the input and output space, with limited computational resources. We first conduct dimension reduction in output space with very high dimensionality (thousands of outputs) using singular value decomposition (SVD) and identify key features. Mapping between inputs and each feature is then considered, and the active subspace methodology is used to capture the relationship in a low-dimensional subspace, where surrogate models are built. A low-dimensional adaptive learning strategy is proposed to improve the surrogate model. The proposed method is demonstrated on an additively manufactured component, with a high-dimensional field output quantity of interest, the residual stress in the part that has spatial variability due to the stochastic nature of multiple input variables, including process variables and material properties. The main contributions of this paper are: (1) Surrogate models are efficiently built in a lower-dimensional space to address the challenge posed by high diemnsionalities in both the input and output space. (2) Adaptive surrogate modeling is proposed with an active learning function considering both exploration and exploitation with limited samples.

2. DIMENSION REDUCTION

2.1. Dimension reduction in the input space

An active subspace is a low-dimensional subspace that consists of important directions in a model's input parameter space (Constantine (2015)). The effective variability in a model output f due to uncertain inputs is predominantly captured along these directions. The directions constituting the active subspace are the dominant eigenvectors of the uncentered covariance matrix:

$$\mathbf{C} = \int_{\Omega} \left(\nabla_{\boldsymbol{\xi}} f\right) \left(\nabla_{\boldsymbol{\xi}} f\right)^{\top} \mu(d\boldsymbol{\xi}) \tag{1}$$

which is a positive semi-definite matrix with $\mu(d\boldsymbol{\xi}) = \pi(\boldsymbol{\xi})d(\boldsymbol{\xi})$, where $\pi(\boldsymbol{\xi})$ is the joint probability density function of $\boldsymbol{\xi}$. Herein, the random vector $\boldsymbol{\xi} \in \Omega \in \mathbb{R}^{N_p}$ is the vector of uncertain model inputs, N_p is the number of the uncertain inputs; f is assumed to be a square integrable function with continuous partial derivatives with respect to the input parameters; further, we assume that the partial derivatives are square integrable. Since $\mathbf{C}$ is

symmetric and positive semi-definite, it admits a spectral decomposition:

$$\mathbf{C} = \mathbf{W}\Lambda\mathbf{W}^{\top} \tag{2}$$

Here, $\Lambda = diag(\lambda_1, \ldots, \lambda_{N_p})$ with the eigenvalues λ_i's sorted in descending order $\lambda_1 \geqslant \lambda_2 \geqslant \ldots \geqslant \lambda_{N_\mathrm{p}} \geqslant 0$. and $\mathbf{W}$ has the (orthonormal) eigenvectors $\mathbf{w}_1, \ldots, \mathbf{w}_{N_p}$ as its columns. The eigenpairs are partitioned about the rth eigenvalue such that $\lambda_r/\lambda_{r+1} \gg 1$,

$$\mathbf{W} = [\mathbf{W}_1\ \mathbf{W}_2], \quad \Lambda = \begin{bmatrix} \Lambda_1 & \\ & \Lambda_2 \end{bmatrix} \tag{3}$$

The columns of $\mathbf{W_1} = [\mathbf{w}_1 \ldots \mathbf{w}_r]$ span the dominant eigenspace of $\mathbf{C}$ and define the active subspace, and Λ_1 is a diagonal matrix with the corresponding set of eigenvalues, $\lambda_1, \ldots, \lambda_r$, on its diagonal. Once the active subspace is computed, dimension reduction is accomplished by transforming the parameter vector $\boldsymbol{\xi}$ into $\boldsymbol{\eta} = \mathbf{W}_1^{\top}\boldsymbol{\xi} \in \mathbb{R}^r$.

2.2. Output dimension reduction by SVD

SVD reduces the dimension by projecting the original data along the first few orthogonal principal directions that capture most of the variance in the data. If $\boldsymbol{X} \in \mathbb{R}^{M\times N}$ then there exists $\boldsymbol{U}$, $\boldsymbol{V}$ and $\boldsymbol{\Sigma}$ such that

$$\boldsymbol{X} = \boldsymbol{U}\boldsymbol{\Sigma}\boldsymbol{V}' = \sum_{k=1}^{\min(M,N)} \sigma_k \mathbf{u}_k \mathbf{v}_k' \tag{4}$$

This factorization is called singular value decomposition. $\boldsymbol{X}$ is a $M \times N$ matrix. $\boldsymbol{U}$ is a $M \times M$ unitary matrix ($\boldsymbol{U}'\boldsymbol{U} = \boldsymbol{U}\boldsymbol{U}' = \boldsymbol{I}_M$) and consists of left singular vectors ($\boldsymbol{U} = [\boldsymbol{u}_1, \boldsymbol{u}_2, \ldots, \boldsymbol{u}_M]$). $\boldsymbol{V}$ is a $N \times N$ unitary matrix ($\boldsymbol{V}'\boldsymbol{V} = \boldsymbol{V}\boldsymbol{V}' = \boldsymbol{I}_N$) and consists of right singular vectors ($\boldsymbol{V} = [\boldsymbol{v}_1, \boldsymbol{v}_2, \ldots, \boldsymbol{v}_N]$). $\boldsymbol{\Sigma}$ is a $M \times N$ rectangular diagonal matrix that consists of singular values $\sigma_1, \sigma_2, \ldots, \sigma_p$, $p = min\{M,\ N\}$ and $\sigma_1 \geqslant \sigma_2 \geqslant \ldots \geqslant \sigma_p$. Per the unitarity of $\boldsymbol{U}$ and $\boldsymbol{V}$ and the properties of matrix production, $\boldsymbol{U}'\boldsymbol{X}\boldsymbol{V} = diag(\sigma_1, \sigma_2, \ldots, \sigma_p)$.

The amount of variance explained by the i-th singular value and corresponding singular vector pairs is given by:

$$R^2_{SVD} = \sigma_i^2/\Sigma_j\sigma_j^2. \tag{5}$$

To build an approximation of the original matrix by using lower dimensional components, perform SVD on the original data, select the top k largest singular values in $\boldsymbol{\Sigma}$ and the corresponding first r columns selected from $\boldsymbol{V}$. An approximation of the original matrix $\boldsymbol{X}$ can be reconstructed by using:

$$\hat{\boldsymbol{X}} = \boldsymbol{U}_r\boldsymbol{\Sigma}_r\boldsymbol{V}_r', \tag{6}$$

where $\boldsymbol{U}_r$ is a matrix containing the first r left singular vector, $\boldsymbol{\Sigma}_r$ is the first r singular values organized in a $r \times r$ diagonal matrix and $\boldsymbol{V}_r$ is a matrix containing the firs r right singular vectors.

The amount of overall variance captured by the reconstructed matrix can be calculated using Eq. (5) and the number of singular values that is used to reconstruct the matrix, r.

A lower dimensional representation (dimension r) in place of the original data (dimension N) can be taken as

$$\hat{\boldsymbol{X}}^{LD} = \boldsymbol{U}_r\boldsymbol{\Sigma}_r, \tag{7}$$

where $\hat{\boldsymbol{X}}^{LD} \in \mathbb{R}^{M\times r}$ contains M r-dimensional points. These points can be viewed as the coordinates on the orthornormal basis $[\boldsymbol{v}_1, \boldsymbol{v}_2, \ldots, \boldsymbol{v}_r]$. We will refer to these coordinates as 'features'. We consider a spatially varying field quantity, $\boldsymbol{S} = \boldsymbol{S}(\boldsymbol{\theta})$, where $\boldsymbol{\theta} \in \boldsymbol{\Omega}$ is the input on its domain $\boldsymbol{\Omega}$. $\boldsymbol{S}(\boldsymbol{\theta}) \in \mathbb{R}^{r\times c}$ is evaluated on a two-dimensional mesh of size $(r \times c)$ for a given set of inputs $\boldsymbol{\theta}$. $\boldsymbol{S}(\boldsymbol{\theta})$ is available at N_s samples, drawn from the joint probability density function of $\boldsymbol{\theta}$. A data matrix $\boldsymbol{X} \in \mathbb{R}^{N_s\times(r\times c)}$ is constructed using the field data at N_s samples, each row of $\boldsymbol{X}$ contains the matrix $\boldsymbol{S}$, reshaped as a row vector of size $(r \times c)$.

We use a matrix $\mathcal{L}$ to denote the features of $\boldsymbol{S}$. $\mathcal{L}$ has N_s rows, each containing feature values corresponding to a sample. The number of columns in $\mathcal{L}$ can be determined by using the amount of explained variance as shown in eq.(5) for the specific engineering problem, i.e., equal to the number of singular vector-singular value pairs (K^*) that is sufficient for reconstructing the field $\boldsymbol{S}$ with desired accuracy. The feature matrix $\mathcal{L}$ can be mathemati-

cally represented as:

$$\mathcal{L} = \begin{bmatrix} \mathcal{L}_{11} & \mathcal{L}_{21} & \cdots & \mathcal{L}_{K^*1} \\ \mathcal{L}_{12} & \mathcal{L}_{22} & \cdots & \mathcal{L}_{K^*2} \\ \vdots & \vdots & \ddots & \vdots \\ \mathcal{L}_{1N_s} & \mathcal{L}_{2N_s} & \cdots & \mathcal{L}_{K^*N_s} \end{bmatrix} \tag{8}$$

Correspondingly, the approximation $\hat{\boldsymbol{S}}$ of $\boldsymbol{S}$ will be each row of the product of the matrices, $\mathcal{L}$ and $\boldsymbol{V}_{K^*}$, reshaped to a matrix of dimension r-by-s. Note that each element $\mathcal{L}_{ji}$ in matrix $\mathcal{L}$ represents a value of a particular feature j corresponding to a sample i. This is an abstract value in the low-dimensional latent space; one such value does not represent any physical value (output in the original high-dimensional space). Each element X_{im} in $\boldsymbol{X}$ represents a physical QoI in the physical space at a particular point m in the mesh of size $r \times c$, corresponding to the sample i of a total size N_s.

3. ACTIVE LEARNING STRATEGY

There are three key components in the proposed active learning for adaptive improvement strategy: the initial training samples, the learning function and the stopping criteria. Two sets of samples are first generated: one for building initial surrogate model, the other is used as a testing set. An active learning function that combines exploration and exploitation will be used to choose new training samples that will be added to the first set for updating the surrogate model in each iteration; the testing set will remain unchanged throughout the active learning process.

The initial set of training samples, $\mathcal{D}_0 = \{(\boldsymbol{\theta}_i, \boldsymbol{S}_i)\}_{i=1}^{N_0}$, is generated using the Latin hypercube sampling (LHS) technique and will be used to construct the initial surrogate model. The testing sample set, $\mathcal{D}_t = \{(\boldsymbol{\theta}_i, \boldsymbol{S}_i)\}_{i=1}^{N_t}$, is also generated using LHS. The active learning function $l(\boldsymbol{\eta})$) is then employed to iteratively add new training samples into $\mathcal{D}_0$ in order to adaptively improve the surrogate model. This learning function has two parts, global exploration part which is multiplied by α and local exploitation part which is timed by $(1-\alpha)$. The exploration part is a distance-based metric for exploring unsampled regions in the domain; the exploitation is a nonlinear measure for identifying regions with large prediction bias. $\alpha \in [0,1]$ is the weighting factor balancing exploration and exploitation.

$$\begin{aligned} l(\boldsymbol{\eta}) = \alpha \times \Bigg(& \frac{w_F \sum_{j=1}^{N} \|\boldsymbol{\eta} - \boldsymbol{\eta}_j^{\text{train},F}\|}{N \cdot \max_{p \neq q} \|\boldsymbol{\eta}_p^{\text{train},F} - \boldsymbol{\eta}_q^{\text{train},F}\|} \\ & + \sum_i \frac{w_i \sum_{j=1}^{N} \|\boldsymbol{\eta}_i - \boldsymbol{\eta}_j^{\text{train},i}\|}{N \cdot \max_{p \neq q} \|\boldsymbol{\eta}_p^{\text{train},i} - \boldsymbol{\eta}_q^{\text{train},i}\|} \Bigg) \\ & + (1-\alpha) \times \frac{\mathcal{R}\left(\boldsymbol{\eta}; \boldsymbol{\eta}_{nr}\right)}{\max\{\mathcal{R}(\boldsymbol{\eta}; \boldsymbol{\eta}_{nr})\}} \end{aligned} \tag{9}$$

The exploration part consists of a single ratio and a sum of ratios. All ratios are multiplied by a weighting factor w_F or w_i, which account for the contributions of different features. For each of the dominant features indexed by $k = 1, 2, \ldots, K^*$, first calculate the ratio of $w_k = \sigma_k^2 / \Sigma_{m=1}^{K^*} \sigma_m^2$ and the mean absolute error of all training points with current surrogate model, MAE_k; then calculate the product $w_k \cdot MAE_k$. The feature with the largest product is referred to as 'focus feature' with corresponding weight w_F; others are referred to as 'non-focus feature'. The numerator quantifies the Euclidean distance between $\boldsymbol{\eta}$, the unknown point and $\{\boldsymbol{\eta}_j^{\text{train},F}\}_{j=1}^{N}$, all active variables corresponding to all N training points (obtained by using $\mathbf{W}_{1F}$, the bases of active subspace associated the focus feature); the denominator is a normalizing factor, which is N times the maximum largest pairwise Euclidean distance among all N training points. The sum of ratios contains ratio of all non-focus features. Because the active subspace associate with each feature is different, the unknown point $\boldsymbol{\eta}$ in the active subspace of the focus feature need to be properly transferred to the active subspace of the corresponding feature i using the matrices $\mathbf{W}_{1F}$ and $\mathbf{W}_{1i}$, $\boldsymbol{\eta}_{1i} = \mathbf{W}_{1i}^{\top} \mathbf{W}_{1F} \cdot \boldsymbol{\eta}$. The exploitation part is defined based on the residual of the current surrogate model prediction such that $\mathcal{R}\left(\boldsymbol{\eta}; \boldsymbol{\eta}_{nr}\right) = \mathcal{L}_F(\boldsymbol{\eta}_{nr}) - \hat{\mathcal{L}}_F(\boldsymbol{\eta}_{nr})$, where $\boldsymbol{\eta}_{nr} \in \{\boldsymbol{\eta}_j^{\text{train},F}\}_{j=1}^{N}$ is the training point with smallest Euclidean distance to the unknown point $\boldsymbol{\eta}$, i.e., nearest neighbor.

The new training sample $\boldsymbol{\theta}^*$ can be obtained in two steps: (1) find the maximizer of the learning function $\boldsymbol{\eta}^* = argmax(l(\boldsymbol{\eta}))$; (2) transfer $\boldsymbol{\eta}^*$ back to the input variables' domain Ω, $\boldsymbol{\theta}^* = \mathbf{W}_{1F}^{\top} \boldsymbol{\eta}^*$. In order to find the maximizer of the learning function

$l(\boldsymbol{\eta})$, sampling-based optimization is adopted here because the learning function that is constructed based on distance calculations between samples. A candidate pool $\mathcal{P}_\eta$ is first generated based on the information provided by the initial surrogate models. The learning function $l(\cdot)$) is then evaluated at each sample within $\mathcal{P}_\eta$, $\boldsymbol{\eta}^*$ and $\boldsymbol{\theta}^*$ is selected. The physics-based model can then be evaluated at $\boldsymbol{\theta}^*$ to obtain $\boldsymbol{S}^*$ and the dataset of all training samples will be updated as $\mathcal{D}_i = \mathcal{D}_{i-1} \bigcup \{(\boldsymbol{\theta}^*, \boldsymbol{S}^*)\}$, where i indicates the iteration. $\boldsymbol{\eta}^*$ should be removed from $\mathcal{P}_\eta$ at iteration i. Finally, the iterative process ends until the predefined stopping criteria, i.e, the accuracy level is achieved. The proposed active learning function balances exploration and exploitation, considers contributions of all dominant features, and provides an easy way to generate high dimensional input samples.

4. NUMERICAL EXAMPLE

Electron beam melting (EBM) is an additive manufacturing (AM) process of fusing powder particles, layer-upon-layer, using an electron beam as the energy source. Multiple passes of a low power electron beam is used for heating and sintering the powder bed prior to selective melting. We focus on the thermo-mechanical behavior of an AM part produced by the EBM process using Ti6Al4V. A finite element-based thermal analysis model is used to simulate the thermal response of the part and a finite element-based mechanical model that uses the part's thermal response to estimate the residual stress in the part at the end of the cooling phase. A layer

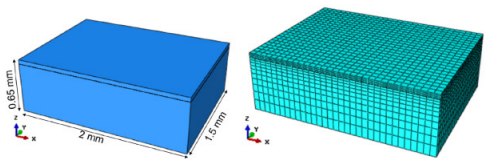

Figure 1: Part geometry and the corresponding mesh as modeled in Abaqus

thickness, 50 µm and a part of dimensions (in mm), $2 \times 1.5 \times 0.65$ is used as shown in Fig. 1 (left). A non-uniform mesh is employed wherein a finer mesh is considered for the powder region where the heat flux is applied as shown in Fig. 1 (right). The mesh consists of 13,200 nodes and 10,752 elements in total.

Surrogate models (one for each dominant feature) are constructed for the residual stress field, $\boldsymbol{S}$ at the cross-section of the part ($x-z$ plane in Fig. 1) passing through its center ($x^c - z^c$ plane). The surrogate model maps three sets of parameters, the process parameters, mechanical properties, and thermal properties to the feature. Process parameters include beam power, scan speed, and pre-heat temperature. Mechanical properties include yield strength, elastic modulus, and bulk density of Ti6Al4V. Thermal properties include specific heat (C_p) and bulk thermal conductivity (κ), which are considered to be functions of the local temperature, T, and a polynomial of degree 2 is fit to a set of data pertaining to the variation of C_p and κ with temperature (20K – 1655K), provided in Fu and Guo (2014). Hence, a total of 12 parameters ($\boldsymbol{\theta}$) are mapped to the stress field. A uniform probability distribution is considered for each parameter with range $[0.9\boldsymbol{\theta}_0, 1.1\boldsymbol{\theta}_0]$, where $\boldsymbol{\theta}_0$ denotes a vector of nominal values, listed in Table 1. An initial set of training samples $\mathcal{D}_0$ and

Table 1: Nominal values of parameters

Scan speed, v	500 mm/s
Beam power, P	160 W
Pre-heat temperature, T_0	650 °C
Yield strength, Y	825 MPa
Density, ρ	4428 kg/m^3
Elastic Modulus, E	110 GPa
C_{0,C_p}, C_{1,C_p}, C_{2,C_p}	540, 0.43, -3.2×10^{-5}
$C_{0,\kappa}$, $C_{1,\kappa}$, $C_{1,\kappa}$	7.2, 0.011, 1.4×10^{-6}

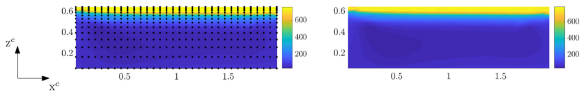

Figure 2: Residual stress field in the $x^c - z^c$ plane

testing samples $\mathcal{D}_t$ are selected using LHS; the number of samples in these sets are N_0 and N_t. Residual stress field is initially computed at the $x^c - z^c$ plane for N_0 samples in the 12-dimensional input domain using the detailed thermal and mechanical models. Stress data is simulated on a 2-dimensional non-uniform grid comprising 32 points along the length

(x^c) and 14 points along the height (z^c) as highlighted in Fig. 2 (left).

4.1. Dimension reduction

In order to address the challenge of the high dimensionalities of both the input and output spaces, the surrogate models will be constructed for in low-dimensional space. Dimension reduction will be performed as stated in Section 2. The number of features to build surrogate models, K^*, is set to three, as the top three feature will account for over 95% of the variance in the QOI; for each feature, $\mathcal{L}_1$, $\mathcal{L}_2$, $\mathcal{L}_3$, a corresponding active subspace is then computed. The number of active variables is set to one for all the features because the variance explained by the first eigenvector, i.e, the first column of $\mathbf{W}$, is over 95%. A linear regression model will be used as the form of the surrogate model. Comparisons of using more than three features, as well as using a larger number of active variables are performed; there is no significant difference than the strategies mentioned in the preceding paragraph. Also note that in all experiments, it is observed that feature 1 is always the focus feature.

4.2. Surrogate models and performance metric

The map from $\boldsymbol{\theta}$ to each feature $\mathcal{L}_j$ is approximated by a surrogate model $\mathcal{L}_j(\boldsymbol{\theta}) = \hat{G}_j(\boldsymbol{\eta}_j)$. The output QOI, $\boldsymbol{S}$, is reconstructed using surrogate prediction for each feature $\mathcal{L}_j$; the reconstructed stress field are denoted using $\hat{\boldsymbol{S}}$. The surrogate model constructed at the i-th iteration is denoted as $\hat{G}_j^i$, $i = 0$ being the initial surrogate model constructed using $\mathcal{D}_0$. At each iteration, the accuracy of surrogate model will be evaluated every sample indexed by $m = 1, 2, \ldots, N_t$ samples in $\mathcal{D}_t$ using the metric based on the relative $l2$-norm of the difference in the prediction of the stress field:

$$\epsilon = \frac{1}{N_t} \Sigma_{m=1}^{N_t} \frac{\|\boldsymbol{S}_m - \hat{\boldsymbol{S}}_m\|}{\|\boldsymbol{S}_m\|} \tag{10}$$

4.3. Investigation of options for adaptive improvement of surrogate models with active learning

For problems with high dimensionalities in both the input and output space, there are many challenges in efficient adaptive improvement of surrogate models with active learning: (1) With limited computational resources, available training samples are limited. (2) The properties of candidate pool for sampling-based optimization of the active learning function, such as the range, need to be considered. (3) At each iteration, the number of samples is different, therefore, there are different options to map the output $\boldsymbol{S}$ to features $\mathcal{L}$ and the associated mapping of the input $\boldsymbol{\theta}$ to active variables $\boldsymbol{\eta}$. (4) The parameter of the active learning function that balances the exploration and exploitation may affect the adaptive improvement process. In this section, we perform multiple trials to address these challenges. In the following investigations, the size of the testing set N_t is set to 10.

4.3.1. The number of training points

We first investigate the influences of both the size of initial training set and the number of newly-added training points in each iteration. Note that in this investigation, options for mapping, candidate pool properties, and parameter in learning function are kept the same for all trials. The size of the initial training set are chosen as N_0 = 13, 20, and 40. The accuracies of initial surrogate models in active subspace are evaluated using the original space error metric, ϵ, as explained above and shown in the table below. For the influence of the number of newly-added samples, we experimented with 1 and 3. With the size of the initial training set $N_0 = 20$, the results are shown in Fig. 3. The difference between the accuracies of the surrogate models when adding one point at each iteration and when adding three points at each iteration was small. Considering limited computational resources, adaptively adding one new point is an optimal choice.

Table 2: Surrogate model accuracy for different N_0

$N_0 = \{\mathcal{D}_0\}$	13	20	40
Error ϵ	17.38%	9.61%	8.23%

4.3.2. Properties of the candidate pool

A sample-based optimization is used to choose new training point, therefore, a pool of candidate points for active variables, $\mathcal{P}_\eta$, need to be constructed. The range of the candidate points in $\mathcal{P}_\eta$

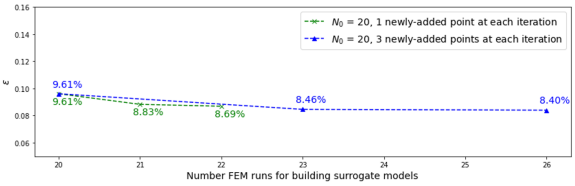

Figure 3: Influence of the number of newly-added samples

should be informed by the range of active variable values corresponding to all N_0 samples in the initial training set $\mathcal{D}_0$. We start with $N_0 = 13$ samples, the range of the active variable values obtained using dimension reduction $\mathcal{R}_{N_0}$ is obtained. Two candidate pools, $\mathcal{P}_\eta^{(1)}$ (much wider than the $\mathcal{R}_{N_0}$, candidates randomly distributed) and $\mathcal{P}_\eta^{(2)}$ (slightly wider than the $\mathcal{R}_{N_0}$, candidates evenly distributed) are generated, as shown in Fig. 4. Note that for candidate pools, only the x-axis values are of interests; they were plotted on y-axis values for easy observation and the y-axis values of the candidates do not have any meanings. The red dots in the figure indicates the lower-dimensional representations of the initial training samples, with y-axis being the first feature $\mathcal{L}_1$ values and x-axis being the active variable values. The red dash is the surrogate of feature 1 trained by $N_0 = 13$ samples and the vertical red dots indicate the range of the active variable of the those samples. Experiments of adaptive improvements of

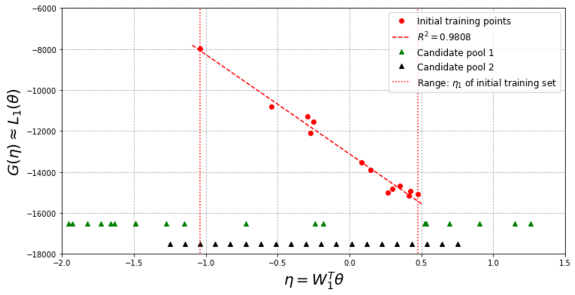

Figure 4: Two candidate pools in active subspace

the surrogate models by using samples both candidate pools are conducted. In each iteration, only one new sample is added to the training set $\mathcal{D}$. The results of the experiments are compared in Fig. 5. The active learning with the wider candidate pool, $\mathcal{P}_\eta^{(1)}$, resulted in lower error at the end.

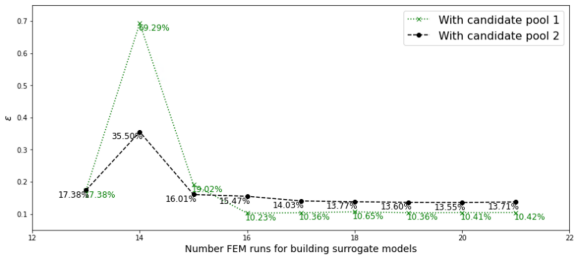

Figure 5: Comparison of using different candidate pool

4.3.3. *Options of mapping*

The number of samples in one iteration is different from that of the previous iteration. Thus in one iteration i (where there are N_i samples for surrogate model construction), the feature can be calculated using the $\boldsymbol{V}$ from the previous iteration (SVD results of iteration $i-1$, denoted as $\boldsymbol{V}^{(i-1)}$), or $\boldsymbol{V}$ in this iteration (denoted as $\boldsymbol{V}^{(i)}$). If $\boldsymbol{V}$ is used, the active variable can be calculated using either $\mathbf{W}_1^{(i-1)}$ (active variable mapping from previous iteration) or $\mathbf{W}_1^{(i)}$ (active variable mapping calculated in this iteration). The options can be summarized in the following flowchart in Fig. 6. We start with $N_0 = 13$ points and candidate pool $\mathcal{P}_1$. The comparison of these three options at the first iteration where the number of samples $N = 14$ is shown in Fig. 7. Note that the newly added point in this iteration is marked in 'x' and the $N_0 = 13$ initial training samples are marked with dots. Surrogate model for feature 1 trained with points obtained by different options are the dashed lines in the corresponding color. We observe that: (1) the feature does not change much whether $\boldsymbol{V}^{(i-1)}$ is used. (2) When active variable values are calculated using $\mathbf{W}_1^{(i)}$, the values are almost identical. Although using the $\boldsymbol{V}^{(i-1)}$ and $\mathbf{W}_1^{(i-1)}$ can result in a better surrogate, it is still recommended to use the feature and active variable mapping at the current iteration.

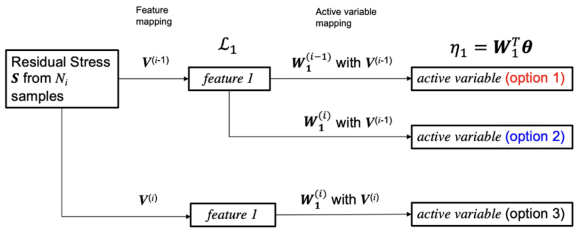

Figure 6: Different mapping options

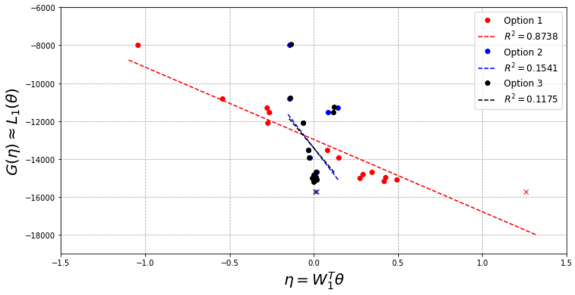

Figure 7: Comparison of different mapping options

4.3.4. Parameter in active learning function

In the active learning function $l(\boldsymbol{\theta})$, the parameter α balances the exploration and exploitation and affect the active learning process in terms of sample selection and the improvement of the surrogate. In this experiment, α = 0, 0.2, 0.5, and 1 are chosen to study the influence of it. We start with N_0 = 13 samples and the results are shown in Fig. 8. Pure exploration (α = 1) yields the best improvement.

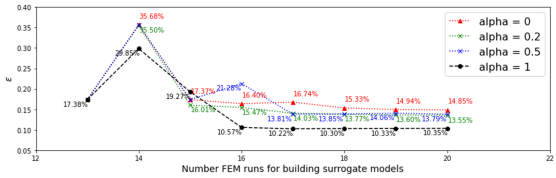

Figure 8: Comparisons of using different α values

5. CONCLUSION

This paper presents a novel approach to efficiently construct and improve surrogate models for high dimensional problems in both the input and output spaces. Principal components and corresponding features of the output are first identified. The active subspace methodology is used to reduce the input dimension. Surrogate models are subsequently built within the reduced spaces, where an active learning strategy is proposed to improve the surrogate model. The adaptive learning is based on the active variables in the low-dimensional space and once the newly-added training sample is selected and can be easily mapped back to the original space for running the physics-based model. The proposed method is demonstrated on an additively manufactured component with a high-dimensional residual stress field and multiple input variables including process variables and material properties. Investigations of different options in the proposed method are conducted.

The adaptive learning strategy proposed in this work is a 'zero-th order' approach in the sense that biases and distance-based metrics are used. In the future, this work can be extended to a 'first-order' based method, in which information directly obtained from the model can be used to guide the active learning process; this is a challenging issue when high dimensionalities and complex multi-physics simulations are involved. In addition, the errors presented in the surrogate modeling process can be quantified, alongside with proper discrepancy modeling either in the low dimensional space or the original high dimensional space, the uncertainty of remaining stress predictions at any location beyond the considered grid can be quantified.

6. REFERENCES

Constantine, P. G. (2015). *Active subspaces: Emerging ideas for dimension reduction in parameter studies*, Vol. 2. SIAM.

Fu, C. and Guo, Y. (2014). "3-dimensional finite element modeling of selective laser melting ti-6al-4v alloy." *2014 International Solid Freeform Fabrication Symposium*, University of Texas at Austin.

Guo, Y., Mahadevan, S., Matsumoto, S., Taba, S., and Watanabe, D. (2022). "Investigation of surrogate modeling options with high-dimensional input and output." *AIAA Journal*, 1–15.

Sacks, J., Schiller, S. B., and Welch, W. J. (1989). "Designs for computer experiments." *Technometrics*, 31(1), 41–47.

Vohra, M., Nath, P., Mahadevan, S., and Tina Lee, Y.-T. (2020). "Fast surrogate modeling using dimensionality reduction in model inputs and field output: Application to additive manufacturing." *Reliability Engineering & System Safety*, 201, 106986.

White, A., Mahadevan, S., Grey, Z., Schmucker, J., and Karl, A. (2019). "Efficient calibration of a turbine disc heat transfer model under uncertainty." *AIAA Propulsion and Energy 2019 Forum*, 4253.